infrastructures

MDPI

Article

Railway Track Loss-of-Stiffness Detection Using Bogie Filtered Displacement Data Measured on a Passing Train

Abdollah Malekjafarian [1,*], Eugene J. OBrien [2], Paraic Quirke [3], Daniel Cantero [4] and Fatemeh Golpayegani [5]

1 Structural Dynamics and Assessment Laboratory, School of Civil Engineering, University College Dublin, D04V1W8 Dublin, Ireland
2 School of Civil Engineering, University College Dublin, D04V1W8 Dublin, Ireland; eugene.OBrien@ucd.ie
3 Murphy Geospatial, Global House, Kilcullen Business Campus, R56K376 Kilcullen, Ireland; pquirke@murphysurveys.ie
4 Department of Structural Engineering, Norwegian University of Science & Technology, 7491 Trondheim, Norway; daniel.cantero@ntnu.no
5 School of Computer Science, University College Dublin, D04V1W8 Dublin, Ireland; fatemeh.golpayegani@ucd.ie
* Correspondence: abdollah.malekjafarian@ucd.ie; Tel.: +353-1-7163207

Abstract: This paper presents an innovative numerical framework for railway track monitoring using acceleration measurements from sensors installed on a passenger train. A numerical model including a 10 degrees of freedom train passing over a three-layer track is employed. The bogie filtered displacement (BFD) is obtained from the bogie vertical acceleration using a numerical integration method and a band-pass filter. The BFD is compared to the filtered track longitudinal profile and can be seen to contain the main features of the track profile. This is also experimentally confirmed using field measurements where an in-service Irish Rail train was instrumented using inertial sensors. The proposed algorithm is employed to find the BFDs from the bogie accelerations. A track level survey was also undertaken to validate the measurements. It is shown that the BFDs from several passes are in good agreement with the surveyed profile. Finally, the BFDs are numerically used to find track defects such as hanging sleepers. The mean of the BFDs obtained from two populations of train passes over a healthy and a damaged track are employed to detect the loss of stiffness at the subgrade layer. The effect of the train forward speed variation and measurement noise are also investigated.

Keywords: railway track; monitoring; drive-by; assessment; hanging sleeper; in-service train

Citation: Malekjafarian, A.; OBrien, E.J.; Quirke, P.; Cantero, D.; Golpayegani, F. Railway Track Loss-of-Stiffness Detection Using Bogie Filtered Displacement Data Measured on a Passing Train. *Infrastructures* **2021**, *6*, 93. https://doi.org/10.3390/infrastructures6060093

Academic Editor: Minwoo Chang

Received: 18 May 2021
Accepted: 16 June 2021
Published: 21 June 2021

1. Introduction

Increasing demand for mass transportation and freight across countries has become an important challenge for developed countries. A modern and sustainable transportation system is a vital component of a developed economy. Railway networks are important components of any such system. For instance, the total length of railway network in the United States is more than 250,000 km [1] and it is still growing fast. In addition, the usage of railway systems is being increased around the world due to its safety and speed. It is very important for railway owners to keep these systems well maintained and operational. A large portion of the railway lines were built many years ago and were not designed for the current traffic [2]. Today, railway systems are subjected to heavier axle loads, faster speeds, and greater frequency. As a result, they are more vulnerable. Therefore, it is important to implement effective health monitoring systems to ensure more effective functioning of railway systems.

Railway tracks are one of the main components of railway systems. They inevitably deteriorate due to the daily traffic [3]. Minimizing the maintenance costs of railway tracks by monitoring and timely intervention is of great interest to railway managers.

Currently two main methods that are used for monitoring of railway tracks: (a) Performing visual inspection based on a fixed schedule (walking the track). This method includes surveying by means of hand-held portable equipment such as tachometers, levelers and digital gauges. This method is expensive to perform frequently and labor intensive when the total length of railway track in a network is considered [4]. It is most effective for major faults that are visually detectable but may not be reliable for other more subtle faults and those that are only apparent during the passage of a train. (b) Using measuring vehicles. In this method, a vehicle, which is normally called a track recording vehicle (TRV), is used to monitor the track condition. In accordance with European safety standards, railway infrastructure owners are obligated to measure the geometric characteristics of the track at a regular frequency in accordance with the EN 13848 standard. This is generally measured using a TRV. The measurements allow the infrastructure owner to plan preventative maintenance on sections of track that are approaching tolerance limits. If any track parameters are outside of these limits, temporary speed restrictions or suspension of train operations may be required. TRVs are specialized vehicles equipped with optical and inertial sensors [5] that travel periodically over the rail network and record geometric parameters of the track. The longitudinal level and alignment of the left and right rail, track gauge, cross level, twist, curvature and curve radius, gradient and position, using GPS, can all be measured using a TRV [5]. Even though they can provide quite accurate data, they are expensive, which limits the frequency of their usage. Moreover, they may disrupt regular services as they do not always travel at the same speed as normal train traffic. Therefore, there is a demand for more effective methods of monitoring railway tracks.

Recent developments in sensing technology and computational power have provided new opportunities to improve railway track monitoring strategies and reduce inspection costs [6,7]. A common practice is the installation of vibration-based sensors on the track and monitoring its dynamic behavior which can be an indicator of defects. For example, Liu et al. [8] proposed a remote network of sensors for track condition monitoring. A network of nodes measuring vertical acceleration and strain were used in this work. Some researchers also employ fiber Bragg grating (FBG) sensors for the monitoring of railway track behavior [9,10]. The direct installation of vibrational sensors on a track usually provides useful information about its condition, but in reality, instrumentation of an entire railway network is hardly feasible and would be inordinately expensive.

However, several studies have been carried out for the monitoring of different components of railway tracks. For example, railway turnouts are among the most critical elements of railway infrastructure, which are particularly exposed to abrasive wear, fatigue, and shape changes [11–13]. Kampczyk [13] proposed the innovative magnetic-measuring squares (MMS) and total station for measuring the geometric center of a turnout for the safety of railway infrastructure. Kaewunruen and Dindar [14] studied the effect of climate change on the service life of rail turnouts. In this study, they adopted a life cycle costing analysis where the total costs of implementing various measures with different consequences and environmental conditions are considered. Kampczyk [15] presented a novel approach for the continuous monitoring of railway tracks on long sections. In this approach, fiber optic sensors are installed on rails to monitor emerging deformations. Klug et al. [16] also proposed a new concept for the monitoring of railway deformations using fiber optic measurements, acknowledging that the condition of the circular curve of a railway track is a critical element of track position monitoring. Kampczyk [17] employed the measurements collected by an MMS to measure the horizontal versines of a rail track curve. The author also showed that these measurements can be used to find the perpendicularity of rail joints and shortenings.

In recent years, several studies have proposed the installation of sensors on a passing train for track health monitoring [18–21] and railway bridge monitoring [22,23] which is called 'drive-by' monitoring. This method does not disrupt normal service and it can provide real time track condition data every time the train passes. Therefore, it can detect developing track defects at an early stage. It is cheap (as it uses cheap sensors e.g.,

accelerometers) and could be installed on all trains, which would obviate the need for expensive TRV vehicles or direct track instrumentation. Several types of sensor, including laser technology [24], camera [25,26], and inertial sensors (accelerometers, gyrometers, etc.) [27], can be employed for drive-by railway track monitoring, although laser sensors tend to be relatively expensive. Some studies [6,28–31] employ drive-by measurements for the monitoring of track components e.g., crossings, joints, turnout frogs, squats, etc. Wei et al. [6] proposed using train axle box measurements for detecting the degradation of a railway crossing over time. Oregui et al. [29] showed that axle box acceleration measurements can be used for the monitoring of bolt tightness of rail joints. Salvador et al. [31] employed axle box measurements for the detection and classification of track parameters such as welded joints, turnout frogs, and squats. Lederman et al. [20] proposed an energy-based method for detecting track changes using acceleration measurements taken from the train cabin. They plotted the energy of acceleration signals measured from several passes of an in-service train and employed a feature detection method to detect track changes over time. Nafari et al. [24] used the relative vertical distance between the rail surface at two points measured from the train to find the track stiffness profile. Such a measurement can be obtained with a rolling deflection measurement system which uses laser measurements. They showed that the local stiffness variations are reflected in the relative measurements.

Several approaches have been proposed using numerical models of train track interaction. Cantero and Basu [32] proposed a method for identifying railway track irregularities using wavelet transforms of responses measured on a train. They used a numerical model of the train passing over the rail profile without considering track stiffness. Quirke et al. [33] proposed using an optimization method to find railway track stiffness variation from acceleration responses measured on a passing train. They modeled the train as a half-car and employed a Winkler model to represent the track stiffness. The method was computationally intensive and did not have the efficiency required to be used in practice. OBrien et al. [34] proposed a similar optimization method for inferring a track longitudinal profile from drive-by measurements generated with a numerical model. They used a 10 degree of freedom (DOF) half-train model passing over a track modeled as a beam resting on a three-layer sprung mass system representing the sleepers, pads, and ballast. OBrien et al. [27] reported on field testing of the numerical method presented in [34]. They employed bogie vertical acceleration and angular velocity measured from an in-service train to find the longitudinal track profile. The proposed method employed the same optimization algorithm as [34], which needs a calibrated vehicle model. The authors compared the inferred track profile with the surveyed profile recorded using a level survey of the unloaded track. The inferred profile showed good consistency and reflected the general shape of the profile, but the amplitude was overestimated. In a similar study, Odashima et al. [35] estimated railway track irregularities from car-body acceleration responses using inverse dynamics. They inferred the track profile using a known vehicle model and acceleration responses measured from an in-service train using the Kalman filtering. Malekjafarian et al. [36] recently employed the Hilbert transform to obtain the instantaneous amplitudes of the acceleration signals measured on a train and proposed a new representation of the signal energy level as a function of train location. A few significant track irregularities were successfully detected, but a number of faults remained undetected and there was no information provided about the fault types.

The main aim of this paper is to use dynamic responses collected on in-service trains for detecting the loss of stiffness in railway tracks. For this purpose, the use of the train bogie vertical displacement for real-time track condition monitoring is proposed. The main hypothesis is that the vertical displacement can be inferred from the vertical acceleration. The train-track interaction is numerically modeled using the finite element (FE) method in Matlab. It is shown that the bogie filtered displacement (BFD) can be obtained using numerical integration of its vertical acceleration and a band-pass filter. It is also shown numerically that the BFD is highly correlated with the track vertical loaded profile. This means that the track condition can be monitored using the BFD, instead of inferring

the profile itself as OBrien et al. [27] and Odashima et al. [35] did. The process of inferring the BFD from its acceleration is experimentally validated using the real data obtained from instrumenting an Irish Rail train in [27]. The BFDs inferred from the double integration process contains the main features of the surveyed profile and are more accurate than the results obtained by OBrien et al. [27]. The potential of the BFD for railway track condition monitoring is also investigated. Several cases of loss-of-stiffness in the track subgrade layer representing hanging sleepers are modeled. It is shown that the track defects can be identified by monitoring BFDs. The influence of train forward speed variation and added noise are also investigated. It is shown that using a population of many train passes can overcome the inaccuracies that may arise from noisy signals and speed variation. Section 2 presents details of the modeling of the train-track interaction. Section 3 introduces the process of inferring BFD from the bogie acceleration and its experimental verification. Section 4 presents the application of BFDs for track fault detection. The results show that the proposed approach can detect the effect of track loss of stiffness, when the responses measured from mean of several passes are used.

2. Numerical Modeling of Track Train Interaction

A numerical track-train interaction (TTI) model similar to that described by Cantero et al. [37] is developed in this paper (Figure 1). TTI is modeled as a coupled system using the finite element (FE) method where the solution is calculated at each time step. The model consists of two subsystems, the train and the track, which interact at the contact points. The details of the numerical modeling of both subsystems is described in this section.

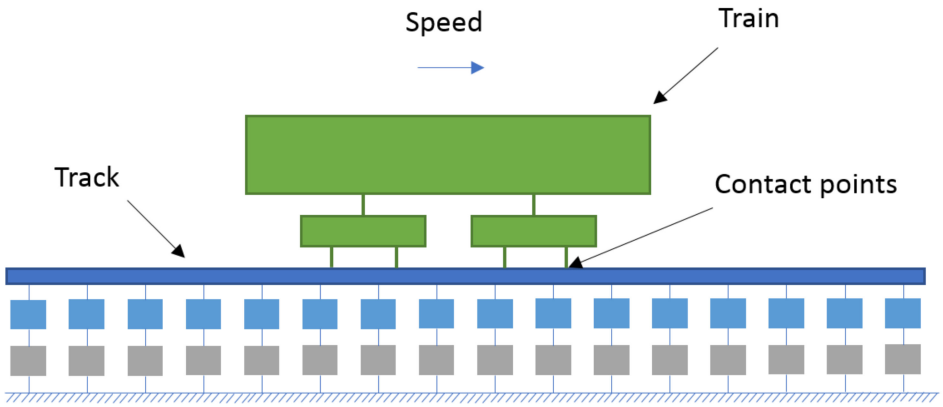

Figure 1. Schematic of the coupled system.

2.1. Track Model

The track is modeled using a beam continuously supported on a three-layer sprung mass system (Figure 2). The beam represents the rail and the layers represents pads, sleepers, ballast, and subgrade systems [37–40]. The rail is modeled as an FE Euler–Bernoulli beam. Each element includes four DOFs, two translational and two rotational. Two beam elements are considered between each pair of sleepers. The beam has constant mass per unit length, m, modulus of elasticity, E, and second moment of area, J. The sprung mass systems are located at regular intervals, L_s, representing the spacing between the sleepers. The properties of the track elements are given in Table 1. The values used in this paper area taken from Zhai et al. [41]. The total length of the track is chosen to be 250 m in this study. This allows the simulations to appropriately model continuous welded rails (CWR) which are normally more than 180 m. To model a more realistic track, a non-uniform subgrade stiffness profile is implemented in the track model. Random stiffnesses are generated using a mean value of 77.5×10^6 N/m and standard deviation of 0.5×10^6 N/m. The distribution of subgrade stiffness is shown in Figure 3. A class 4 track profile is generated using random vertical irregularity according to the US Federal Railroad

Administration (FRA) guideline. It represents a conventional rail surface condition, which is generated using its power spectral density (PSD) function [33,42].

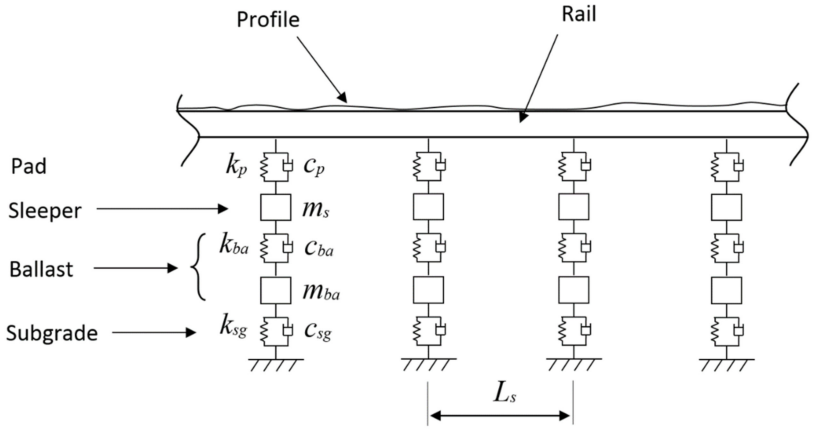

Figure 2. Track model.

Table 1. Properties of the track.

Property	Unit	Value
Elastic modulus of rail	N/m^2	2.059×10^{11}
Rail cross-sectional area	m^2	7.69×10^{-3}
Rail second moment of area	m^4	3.217×10^{-5}
Rail mass per unit length	kg/m	60.64
Rail pad stiffness	N/m	6.5×10^7
Rail pad damping	Ns/m	7.5×10^4
Sleeper mass (half)	kg	125.5
Sleeper spacing	m	0.545
Ballast stiffness	N/m	137.75×10^6
Ballast damping	Ns/m	5.88×10^4
Ballast mass	kg	531.4
Subgrade stiffness mean	N/m	77.5×10^6
Subgrade damping	Ns/m	3.115×10^4

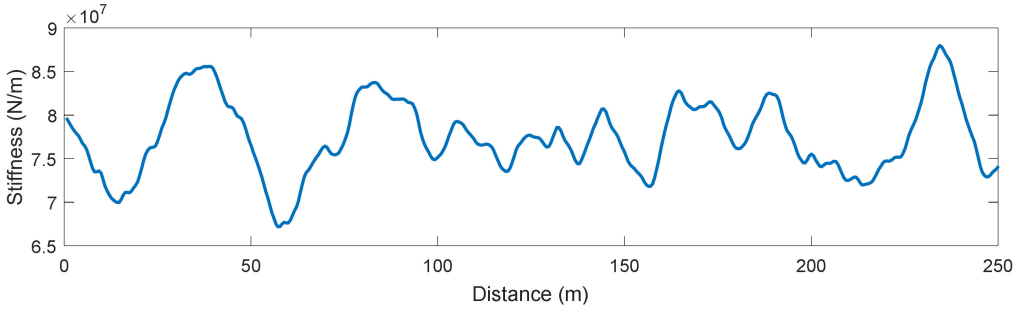

Figure 3. Distribution of subgrade stiffness.

The responses of the track model to moving time-varying forces (interaction forces) are given by the track equations of motion:

$$M_t\ddot{y}_t + C_t\dot{y}_t + K_t y_t = f_{int} \quad (1)$$

where M_t, C_t, and K_t are the mass, damping and stiffness matrices of the track model and $\ddot{y}_t$, $\dot{y}_t$, and y_t are the respective vectors of the track nodal accelerations, velocities, and displacements. The vector, f_{int}, contains the time-varying dynamic interaction forces between the train and track at their contact points.

2.2. Train Model

The train is represented by a two-dimensional car vehicle model (Figure 4). This configuration is well known in the literature and has been used in many studies [42–44]. It consists of 10 DOFs including four vertical translational DOFs for the wheelsets, two vertical translational and two rotational DOFs about each center of gravity of the bogies and vertical translational and rotational DOFs of the main body. m_w represents the masses of the wheelsets, m_b and J_b represent the bogie mass and moment of inertia, m_v and J_v define the body mass and moment of inertia. The wheelsets are connected to the bogies through the primary suspension systems consisting of springs, k_p, and viscous dampers, c_p.

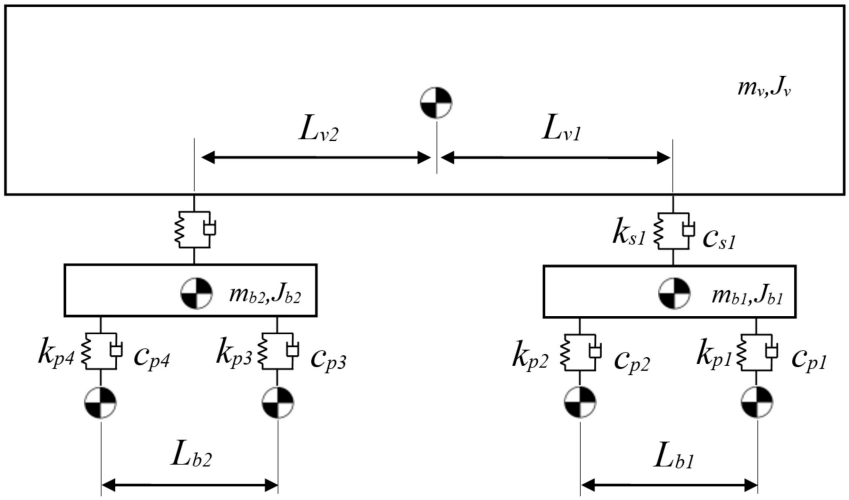

Figure 4. Train model.

The bogies are connected to the main body through the secondary suspension systems consisting of springs, k_s, and a viscous dampers, c_s. The train properties are taken from [45] and are given in Table 2.

Table 2. Properties of the train.

Property	Symbol	Unit	Value
Wheelset mass	m_w	kg	1800
Bogie mass	m_b	kg	3500
Car body mass	m_v	kg	47,800
Moment of inertia of bogie	J_b	kg.m^2	1715
Moment of inertia of main body	J_v	kg.m^2	1.96×10^6
Primary suspension stiffness	k_p	N/m	2.4×10^6
Secondary suspension stiffness	k_s	N/m	0.7×10^6
Primary suspension damping	c_p	Ns/m	20×10^3
Secondary suspension damping	c_s	Ns/m	40×10^3
Distance between car body center of mass and bogie pivot	L_{v1}, L_{v2}	m	8.6875
Distance between axles	L_{b1}, L_{b2}	m	2.5

The equations of motion of the train are represented by the second order differential equations:

$$M_v\ddot{y}_v + C_v\dot{y}_v + K_v y_v = f_{int} \quad (2)$$

where M_v, C_v, and K_v are the mass, damping, and stiffness matrices of the train, respectively and $\ddot{y}_v$, $\dot{y}_v$, and y_v are the vectors of nodal acceleration, velocity, and displacement, respectively.

2.3. Interaction

The train and track are combined together at the wheelsets to form a coupled TTI model. Combining Equations (1) and (2), the coupled equations of motion of the complete model are defined in terms of block matrices:

$$\begin{bmatrix} M_v & 0 \\ 0 & M_t \end{bmatrix} \begin{Bmatrix} \ddot{y}_v \\ \ddot{y}_t \end{Bmatrix} + \begin{bmatrix} C_v & C_{v,t} \\ C_{t,v} & C_t \end{bmatrix} \begin{Bmatrix} \dot{y}_v \\ \dot{y}_t \end{Bmatrix} + \begin{bmatrix} K_v & K_{v,t} \\ K_{t,v} & K_t \end{bmatrix} \begin{Bmatrix} y_v \\ y_t \end{Bmatrix} = F \quad (3)$$

where M_v, C_v, and K_v are coupled mass, damping, and stiffness matrices, respectively, and F is the coupled force vector of the system. The vector F contains the time-varying interaction forces applied by the train to the track. The coupled matrices are recalculated at each time step based on the vehicle's location. The DOFs of the vehicle are merged with those of the track at the connecting points at the wheelsets. The static forces resulted from gravity and the excitations due to the rail irregularities are considered in the force vector. The equations of motion are solved using the Wilson-θ numerical integration scheme. A value of θ = 1.420815 is used to ensure unconditional stability of the algorithm.

3. Track Longitudinal Profile and BFD

3.1. Bogie Filtered Displacement

The train is simulated passing over the track at a speed of 135 km/h. The rail deflection under the first wheel is calculated at a moving coordinate as the train moves forward. Figure 5 compares the unloaded and loaded profiles versus the distance traveled by the train. The unloaded profile is the rail elevation when there is no train on the track. The loaded profile, on the other hand, is the rail deflection under the first wheel of the train. The difference is the deflection of the track due to the axle load of the train which includes static and dynamic components of deflection.

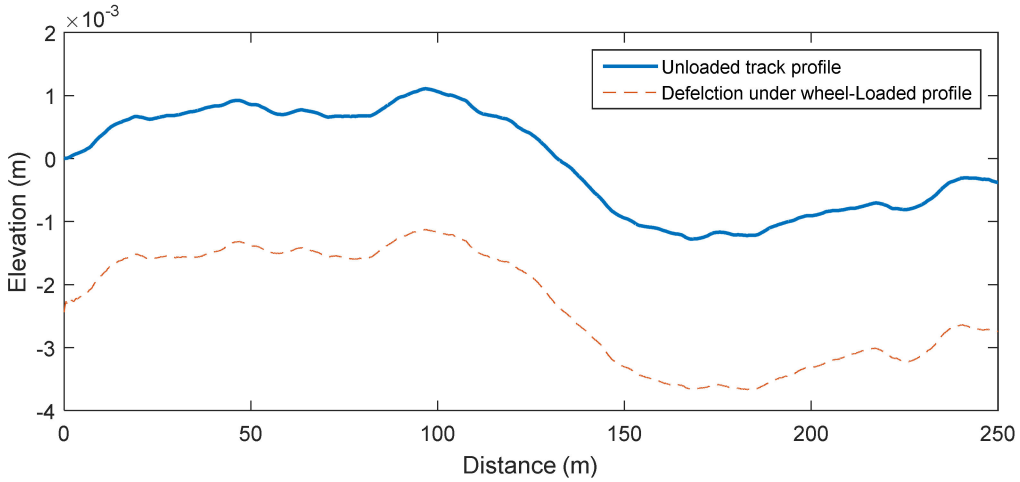

Figure 5. Comparison of the track unloaded and loaded profiles.

The bogie acceleration is also calculated using the FE model. It is assumed that only an accelerometer is installed at the center of mass of the first bogie to measure the bogie vertical acceleration. As acceleration is its second derivative, displacement can be calculated by double integration. However, in practice, accelerations are measured at a specified sampling frequency. In this case, displacement is calculated using a numerical integration

method. It is generally accepted that the displacement calculated with this method is sensitive to measurement noise and other inaccuracies. In most cases, there is drift and some features of displacement associated to low frequency ranges are miscalculated. The bogie displacement drifts and its high frequency components are not of interest in this study and can be removed from the response using a band-pass filter. It will be shown that the filtered displacements contain the main features of the track which are required for track monitoring. OBrien et al. [27] showed that the effects of sleeper spacing, drift, temperature, and measurement noise can be removed from the data by using a band-pass filter. The bogie filtered displacement (BFD) is calculated from the bogie vertical acceleration using the process shown in Figure 6. First the measured acceleration is filtered using a sixth-order Butterworth band-pass filter using a 1–25 Hz band and then the bogie vertical velocity is calculated using a trapezoidal integration scheme. As some new numerical error may be created from the numerical integration, the signal is filtered again using the same filter. Finally, the BFD is calculated using a second numerical integration.

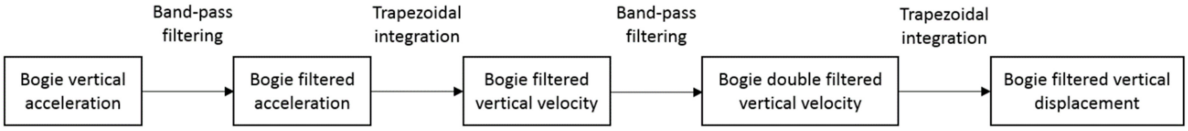

Figure 6. The integration process.

Figure 7 compares the BFD with the unloaded and loaded profiles which are also filtered using the same filter. It can be seen that drifts in the responses are removed and only their relative oscillations are compared. It also shows that the BFD matches the filtered loaded profile reasonably well and contains its main features, showing the potential of BFD for the track health monitoring.

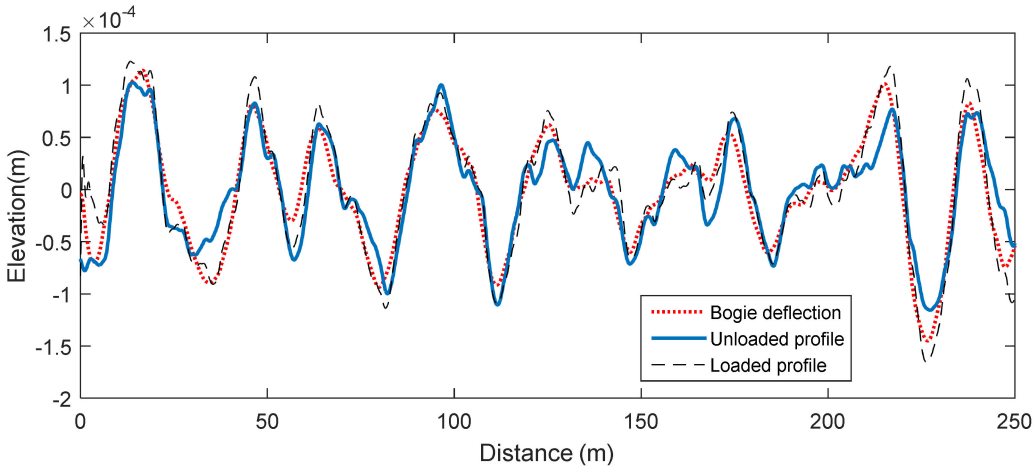

Figure 7. Comparison of BFD to filtered loaded and unloaded profiles.

3.2. Experimental Verification

Although the process explained above provides good accuracy in numerical simulation, its practical application needs to be confirmed. In this section, the process of inferring the BFD from the bogie's acceleration is validated using experimental data. A train owned by Irish Rail (Figure 8a) was instrumented using inertial sensors. A tri-axial accelerometer and a tri-axial gyrometer were installed on the bogie of the train as shown in Figure 8b. The properties of the sensors are given in Table 3. The measurements were taken when the train was in operation on the Dublin-Belfast line from 13th January to 3rd February 2016. This route was upgraded to continuous welded rails in 2000. The bogie responses were measured at a scanning frequency of 500 Hz. A GPS system was also installed on the train to record its location at a frequency of 5 Hz.

(**a**) (**b**)

Figure 8. The measurement set up: (**a**) the train, (**b**) the instrumentation.

Table 3. Properties of sensors.

Sensor Location	Type	Name	Range
Bogie–Bounce	Triaxial Accelerometer	Disynet-DA3802-015g	±15 g
Bogie–Pitch	Triaxial Gyrometer	Crossbow VG400CC-200	±200°/s

Figure 9 shows the bogie acceleration responses from five runs over the same distance of track. As explained in the previous sub-section, there are some variations in the amplitude of the signals due to train forward speed variations and also vehicle loading condition.

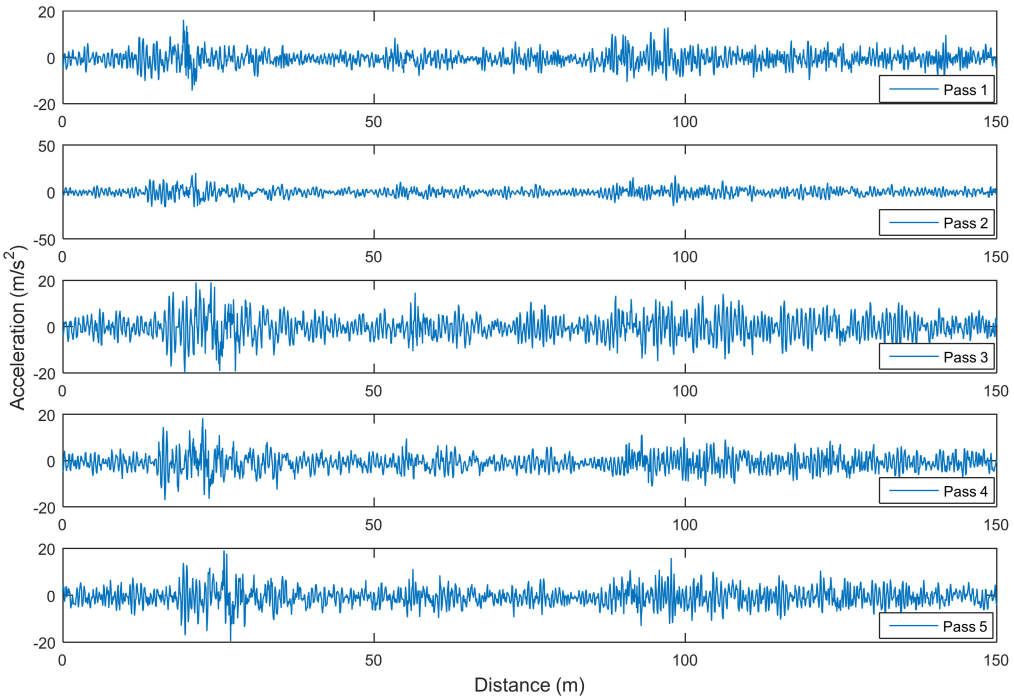

Figure 9. Bogie vertical acceleration signals.

Irish Rail carried out a level survey on the northbound line in this section of track in January 2016. The track longitudinal elevation profile was measured as the average of the elevations from the right and left rails. This was done to characterize the unloaded longitudinal profile through the test section. In this paper, the surveyed profile is filtered using a band-pass filter in the 1–25 Hz frequency range as shown in Figure 10. The accelerations

responses from five passes shown in Figure 9 are used to calculate the BFDs which are compared to the filtered surveyed profile in Figure 10. It can be seen that most of the predominant track features are detected in the inferred bogie responses. There are variations in the elevation values at peaks which can be explained in a number of ways. The surveyed track profile was measured when the track was unloaded, while the train measurements were taken in a loaded condition. As shown in Figure 7, the numerical results confirm that the BDF can be expected to be slightly different from the filtered unloaded profile. In addition, the train forward speed varies for different passes. This speed variation influences the dynamic interaction between the train and the track. Therefore, some changes in the bogie deflection are expected between passes due to speed variation. Furthermore, the mass of the train varies between passes due to differences in the number of passengers, the quantity of fuel and waste. This load variation is a source of change in the BFD extracted from the bogie acceleration. Nevertheless, the inferred data show good repeatability detecting the track elevation features. In order to compare the results with the literature, the inferred BFDs are also compared to the result obtained by OBrien et al. [27] using the same site and data. It can be seen that the BFDs provide higher accuracy compared to their result.

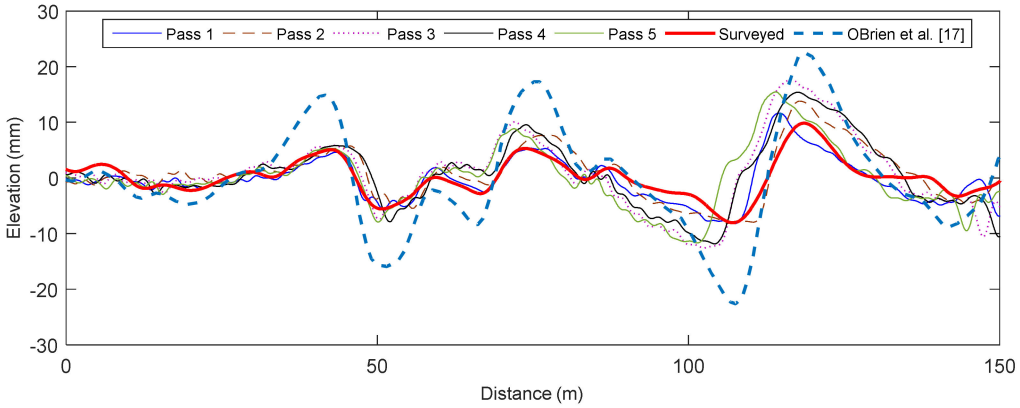

Figure 10. Five passes of BFD and the filtered surveyed (unloaded) profile.

4. Track Condition Monitoring Using the BFD

4.1. Loss of Stiffness at Subgrade Layer

During the passage of a train over a track, a source of ground vibration is related to the variability of the track and ground [46]. The track variability may create local stress concentration under the sleepers. This could lead to a loss of stiffness under the sleeper and a soft soil formation in the subgrade layer. In the long-term, it may create a loss of contact between the ballast and the sleepers, so-called hanging sleepers [46]. If hanging sleepers are not detected at the right time, they may accelerate the track deterioration and cause more damage. In this section, the numerical model is employed to show the potential of the BFD for detecting hanging sleepers. In the numerical model, the subgrade stiffnesses under two sleepers are reduced by 80% at a distance of 120 m from start of the modeled segment. The train is simulated to pass over the damaged track at a speed of 135 km/h. The unloaded track profile and the bogie vertical displacements for the healthy and damaged cases are compared in Figure 11a. Two 'bumps' can be seen in the bogie displacement for the damaged case at the location of the hanging sleepers. These correspond to the passage of the two wheels. Figure 11b shows the filtered version of Figure 11a. The effects of hanging sleepers are amplified by the filtering process. The filtering of the low frequency ranges (under 1 Hz) removes the displacement drift. It can be concluded that the BFD shows good potential for detecting hanging sleepers.

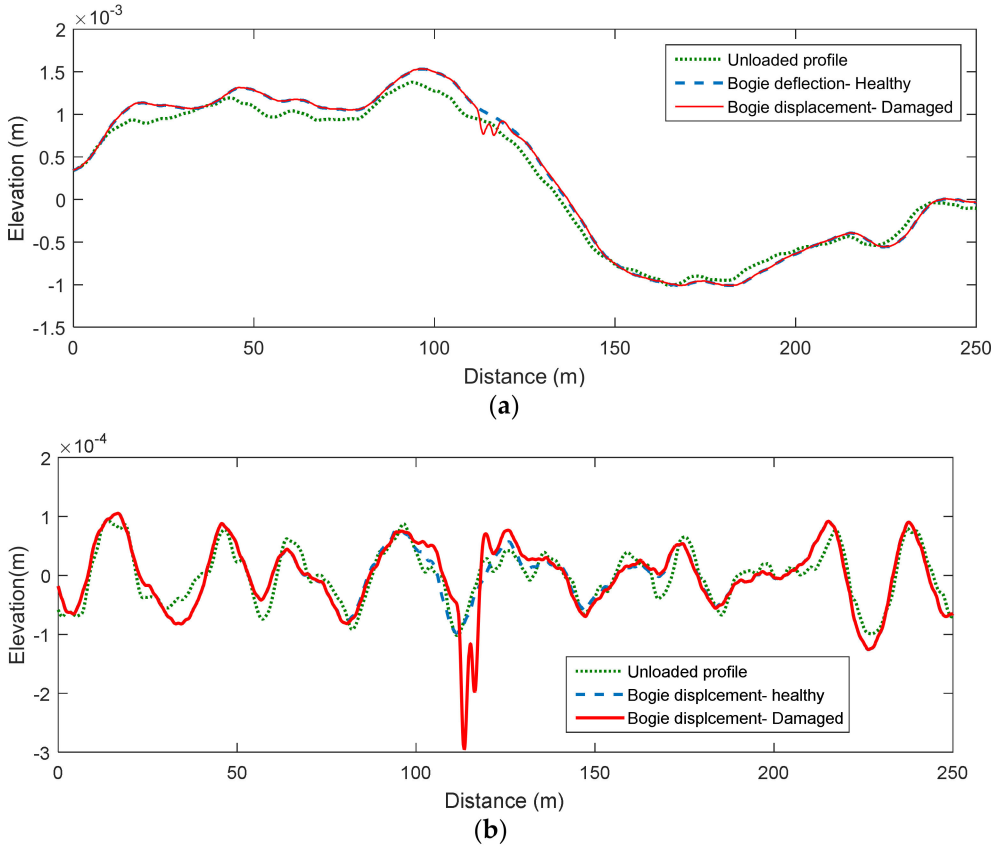

Figure 11. Bogie vertical displacement for the healthy and damaged cases and the unloaded profile, (**a**) unfiltered; (**b**) filtered unloaded profile.

4.2. Multiple Runs in the Presence of Noise

In Section 4.1, the loss of stiffness at the subgrade layer is detected for an ideal case in which there is no noise and the vehicle speed is kept constant. In practice, there is noise in the measurements. In this section, white noise is added to the acceleration signals to generate a more realistic scenario, with the following equation:

$$a_{pol} = a_{calc} + E_p N_{noise} \sigma(a_{calc}) \quad (4)$$

where a_{pol} is the polluted acceleration signal, E_p is the noise level, N_{noise} is a normally distributed vector with a unit standard deviation, a_{calc} is the calculated acceleration signal obtained from the FE simulation, and $\sigma(a_{calc})$ is its standard deviation. The noise level is chosen to be 10% in this study, which is generally considered to be a high noise level.

In addition, the train's forward speed varies for several reasons e.g., driver behavior, restrictions due to track condition. Here, the train speed is randomly generated using a normal distribution with mean of 135 km/h and standard deviation of 15 km/h. Two populations of train passes are created using noisy measurements and with variable train speed for the healthy and another for the damaged case. Figure 12 shows histograms of the vehicle forward speeds used for the two cases.

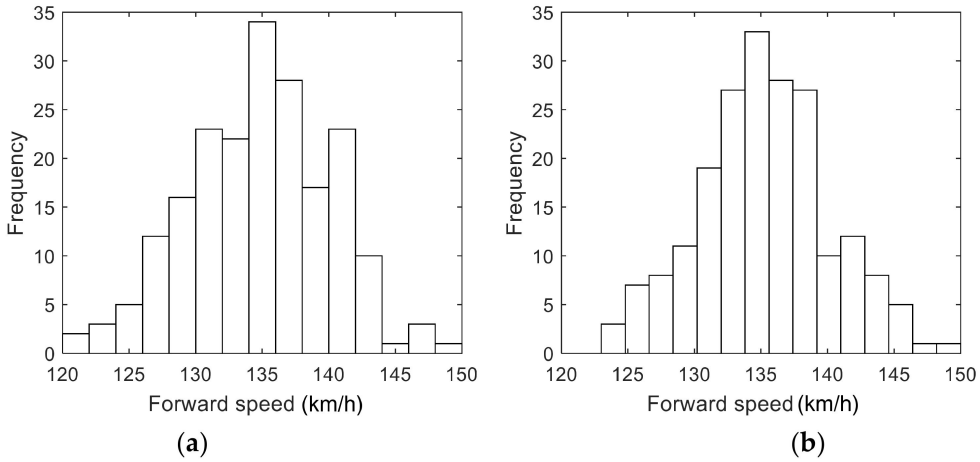

Figure 12. Train speeds, (**a**) healthy case, (**b**) damaged case.

Figure 13a shows the BFDs inferred using the process explained in Figure 5 for the first five train passes over the healthy track. There are large variations in the inferred BFD signals, which are due to the speed variation and measurement noise. The speed variation influences the dynamic interaction between the track and train, which results in different dynamic responses. The numerical trapezoidal integration method is also sensitive to the added noise. Therefore, the inferred signals show large variations in amplitudes. But it can be seen that the BFDs follow similar trends which contain the main features of the loaded track. It means that although individual responses may reveal limited information about the track condition, inferred responses from a population of passes can provide a consistent trend. Figure 13b shows the inferred BFDs from 200 passes over the healthy and damaged tracks. The signals are plotted using transparent colors to show the intensity of the responses versus distance. The damaged location is detectable by comparing populations of the BFDs for the healthy and damaged cases around 120 m. Figure 13c,d shows the tolerance band between the upper and lower tolerance limits for the healthy and damaged cases, respectively. The means of the 200 BFDs in each case are also shown, which can be used as a damage indicator.

In order to investigate the performance of the algorithm for various damage severities, 30%, 50%, and 80% loss of stiffness over one and two sleepers are implemented using the numerical model. Two hundred passes are simulated over each case and the mean is plotted in Figure 14. Figure 14a shows the BFD when only one sleeper is damaged. In this case, 30% loss of stiffness is hardly detectable and it might be masked by the BFD fluctuations. Further, 50% loss of stiffness is more clear in the inferred BFD and 80% is clearly detectable. Figure 14b shows the results for loss of stiffness over two sleepers. In this case, all the BFDs clearly show the loss of stiffness.

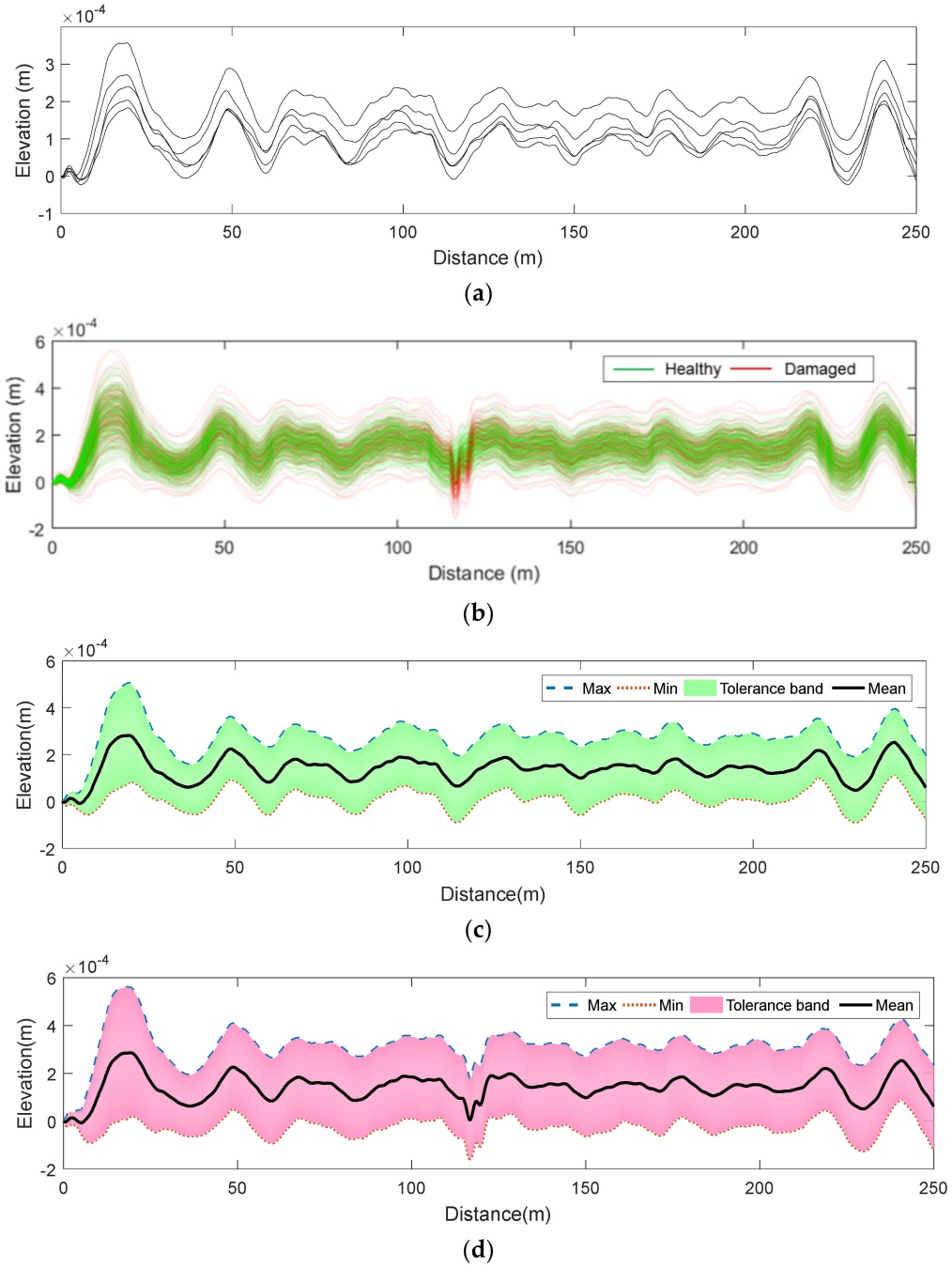

Figure 13. (**a**) The BFDs for the first five passes on the healthy track, (**b**) the BFDs for the populations of passes for the healthy and damaged cases, (**c**) the mean and tolerance band of the healthy population, and (**d**) the mean and tolerance band for the damaged population.

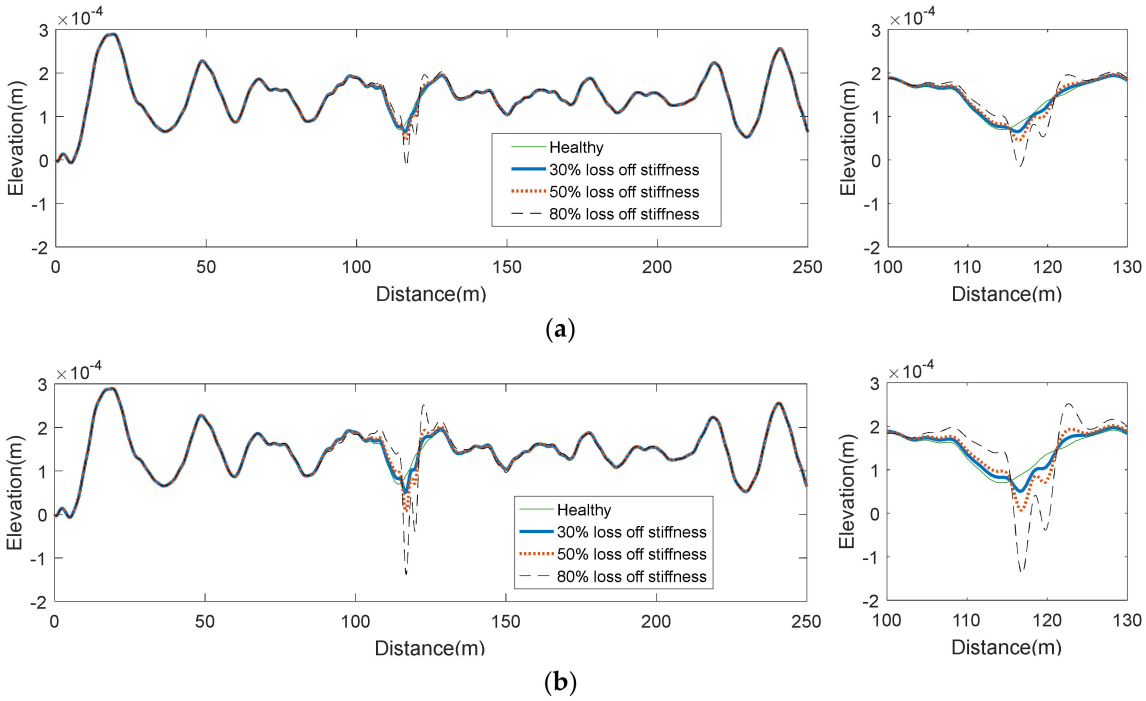

Figure 14. The mean of BFDs for the healthy and damaged tracks, (**a**) for one damaged sleeper, (**b**) for two damaged sleepers.

5. Discussion

This paper presents an innovative approach for detecting loss-of-stiffness using the dynamic responses measured on the bogie on an in-service train. In Section 3, it is shown that the so-called bogie filtered displacement (BFD) can be obtained from the bogie vertical acceleration using a double integration process. The numerical results in this section show that the BFD exhibits similar features to the track vertical loaded profile (Figure 7). This confirms that the bogie vertical acceleration has the potential to be used for track monitoring purposes. Compared to the approaches that are currently being used (e.g., visual inspection or using a TRV vehicle), the proposed approach is more practical as it reveals the track condition under real loading. This is extremely beneficial for the detection of the track loss-of-stiffness, which can only be detected when it is loaded.

The process of obtaining the BFD is experimentally validated using real measurements, as described in Section 3.2. An in-service train was instrumented, and the bogie vertical acceleration was measured using inertial sensors. The BFD obtained from the bogie acceleration is compared with results from the literature and the survey data provided by Irish Rail (Figure 10). This experimentally confirms the potential of BFD for track monitoring, especially when the track condition under real loading is needed.

In Section 4, the potential of BFD for the detection of track loss-of-stiffness is studied. The BFD is inferred from multiple train runs using numerical simulation. It is shown that the unloaded track profile does not reveal the track loss-of-stiffness (Figure 11), while the BFD is sensitive to it at its location. However, the BFD could be misleading when the results from individual runs are compared due to speed variation and the filtering process. To overcome this issue, it is recommended to employ the dynamic responses measured from a population of passes. The results in Figure 14 confirm that the proposed approach can detect the location of hanging sleepers when one or two sleepers are affected.

Among the recent works reported in the literature, which have used measurements collected from in-service trains, most of them have focused on the detection of track faults such as rail irregularities or damage that can be detected using visual inspection. This paper, on the other hand, focuses on damage at the sub-grade layers. In addition, the proposed approach is unique because the track soil layers are evaluated in the loaded condition. Even though this paper shows promising results for the detection of track loss-of-stiffness,

future studies should include the use of real measurements from a damaged railway track e.g., one or two hanging sleepers. In addition, the influence of the train forward speed must be investigated in greater detail.

6. Conclusions

In this paper, the idea of drive-by railway track monitoring is investigated using a train track interaction model. It is shown that the bogie filtered displacement (BFD) can be numerically obtained from the measured acceleration. The band-pass filter removes the high frequency components of the bogie displacement and the drifts. It is demonstrated that the BFD reflects the important features of the railway track loaded profile and can be used for track condition monitoring. The numerical results are confirmed by real measurements from an in-service Irish rail train which is instrumented using accelerometers installed on the train bogie. It is shown that the BFD is sensitive to train forward speed and measurement noise. But when the mean of several passes with different forward speeds is used, the effect of track loss of stiffness can be detected.

Author Contributions: Conceptualization, A.M. and E.J.O.; methodology, A.M. and F.G.; formal analysis, A.M. and F.G.; data curation, D.C. and P.Q.; writing—original draft preparation, A.M., E.J.O. and F.G.; writing—review and editing, A.M., E.J.O. and F.G.; supervision, E.J.O. All authors have read and agreed to the published version of the manuscript.

Funding: The data used in this paper was recorded as part of the Marie Curie Initial Training Network (ITN) action FP7-PEOPLE-2013-ITN. The project has received funding from the European Union's Seventh Framework Programme for research, technological development and demonstration under grant agreement number 607524.

Institutional Review Board Statement: Not applicable.

Informed Consent Statement: Not applicable.

Data Availability Statement: Not applicable.

Conflicts of Interest: The authors declare no conflict of interest.

References

1. Available online: https://erail.in/blog/countries-with-largest-railway-networks-in-world/50 (accessed on 21 June 2021).
2. Gunn, D.A.; Chambers, J.E.; Dashwood, B.E.; Lacinska, A.; Dijkstra, T.; Uhlemann, S.; Swift, R.; Kirkham, M.; Milodowski, A.; Wragg, J.; et al. Deterioration model and condition monitoring of aged railway embankment using non-invasive geophysics. *Constr. Build. Mater.* **2018**, *170*, 668–678. [CrossRef]
3. Kaewunruen, S.; Remennikov, A.M. Field trials for dynamic characteristics of railway track and its components using impact excitation technique. *NDT E Int.* **2007**, *40*, 510–519. [CrossRef]
4. Malekjafarian, A.; OBrien, E.J.; Golpayegani, F. Indirect monitoring of critical transport infrastructure: Data analysis and signal processing. In *Data Anlytics Applications for Smart Cities*; Alavi, A.H., Buttlar, W.G., Eds.; Auerbach/CRC Press: Boca Raton, FL, USA, 2018.
5. Berggren, E.G.; Nissen, A.; Paulsson, B.S. Track deflection and stiffness measurements from a track recording car. *Proc. Inst. Mech. Eng. Part F J. Rail Rapid Transit* **2014**, *228*, 570–580. [CrossRef]
6. Wei, Z.L.; Nunez, A.; Li, Z.L.; Dollevoet, R. Evaluating Degradation at Railway Crossings Using Axle Box Acceleration Measurements. *Sensors* **2017**, *17*, 2236. [CrossRef]
7. Barke, D.; Chiu, W.K. Structural health monitoring in the railway industry: A review. *Struct. Health Monit.* **2005**, *4*, 81–93. [CrossRef]
8. Liu, C.; Wei, J.H.; Zhang, Z.X.; Liang, J.S.; Ren, T.Q.; Xu, H.Q. Design and evaluation of a remote measurement system for the online monitoring of rail vibration signals. *Proc. Inst. Mech. Eng. Part F J. Rail Rapid Transit* **2016**, *230*, 724–733. [CrossRef]
9. Mennella, F.; Laudati, A.; Esposito, M.; Cusano, A.; Cutolo, A.; Giordano, M.; Campopiano, S.; Breglio, G. Railway monitoring and train tracking by fiber Bragg grating sensors. *Proc. SPIE* **2007**, *6619*. [CrossRef]
10. Kerrouche, A.; Boyle, W.J.O.; Gebremichael, Y.; Sun, T.; Grattan, K.T.V.; Taljsten, B.; Bennitz, A. Field tests of fibre Bragg grating sensors incorporated into CFRP for railway bridge strengthening condition monitoring. *Sens. Actuator A Phys.* **2008**, *148*, 68–74. [CrossRef]
11. Jönsson, J.; Arasteh Khouy, I.; Lundberg, J.; Rantatalo, M.; Nissen, A. Measurement of vertical geometry variations in railway turnouts exposed to different operating conditions. *Proc. Inst. Mech. Eng. Part F J. Rail Rapid Transit* **2016**, *230*, 486–501. [CrossRef]

12. Sae Siew, J.; Mirza, O.; Kaewunruen, S. Torsional effect on track-support structures of railway turnouts crossing impact. *J. Transp. Eng. Part A Syst.* **2017**, *143*, 06016001. [CrossRef]
13. Kampczyk, A. Measurement of the geometric center of a turnout for the safety of railway infrastructure using MMS and total station. *Sensors* **2020**, *20*, 4467. [CrossRef]
14. Kaewunruen, S.; Dindar, S. The Effect of Climate Change on Service Life and Cost Investigation of Rail Turnouts with Various Mitigation Methods. In *Inter-Noise and Noise-Con Congress and Conference Proceedings*; Institute of Noise Control Engineering: Reston, VA, USA, 2018; pp. 6091–6101.
15. Kampczyk, A. Railway Special Grid in Near Field Communication Technology for Rail Transport Infrastructure. In *Transport Development Challenges in the 21st Century: Proceedings of the 2019 TranSopot Conference*; Springer Nature: Berlin/Heidelberg, Germany, 2021; p. 87.
16. Klug, F.; Lackner, S.; Lienhart, W. Monitoring of railway deformations using distributed fiber optic sensors. In Proceedings of the Joint International Symposium on Deformation Monitoring (JISDM), Vienna, Austria, 30 March–1 April 2016.
17. Kampczyk, A. Magnetic-Measuring Square in the Measurement of the Circular Curve of Rail Transport Tracks. *Sensors* **2020**, *20*, 560. [CrossRef]
18. Bocciolone, M.; Caprioli, A.; Cigada, A.; Collina, A. A measurement system for quick rail inspection and effective track maintenance strategy. *Mech. Syst. Signal Process.* **2007**, *21*, 1242–1254. [CrossRef]
19. Molodova, M.; Li, Z.L.; Dollevoet, R. Axle box acceleration: Measurement and simulation for detection of short track defects. *Wear* **2011**, *271*, 349–356. [CrossRef]
20. Lederman, G.; Chen, S.H.; Garrett, J.; Kovacevic, J.; Noh, H.Y.; Bielak, J. Track-monitoring from the dynamic response of an operational train. *Mech. Syst. Signal Process.* **2017**, *87*, 1–16. [CrossRef]
21. Malekjafarian, A.; OBrien, E.J.; Cantero, D. Railway track monitoring using drive-by measurements. In Proceedings of the Fifteenth East Asia-Pacific Conference on Structural Engineering and Construction (EASEC-15), Xi'an, China, 11–13 October 2017.
22. Fitzgerald, P.C.; Malekjafarian, A.; Cantero, D.; OBrien, E.J.; Prendergast, L.J. Drive-by scour monitoring of railway bridges using a wavelet-based approach. *Eng. Struct.* **2019**, *191*, 1–11. [CrossRef]
23. Bowe, C.; Quirke, P.; Cantero, D.; O'Brien, E.J. Drive-by structural health monitoring of railway bridges using train mounted accelerometers. In Proceedings of the 5th ECCOMAS Thematic Conference on Computational Methods in Structural Dynamics and Earthquake Engineering, Crete Island, Greece, 25–27 May 2015.
24. Nafari, S.F.; Gul, M.; Roghani, A.; Hendry, M.T.; Cheng, J.J.R. Evaluating the potential of a rolling deflection measurement system to estimate track modulus. *Proc. Inst. Mech. Eng. Part F J. Rail Rapid Transit* **2018**, *232*, 14–24. [CrossRef]
25. Bar-Am, M. On-Train Rail Track Monitoring System. U.S. Patents US8942426B2, 27 January 2015.
26. Fosburgh, B.A.; Nichols, M.E.; Holmgren, P.M.; Larsson, N.T. Railway Track Monitoring. US Patents US20120274772A1, 7 November 2017.
27. OBrien, E.J.; Quirke, P.; Bowe, C.; Cantero, D. Determination of railway track longitudinal profile using measured inertial response of an in-service railway vehicle. *Struct. Health Monit.* **2017**, *17*, 1425–1440. [CrossRef]
28. Zemp, A.; Muller, R.; Hafner, M. Characterization of Train-Track Interactions based on Axle Box Acceleration Measurements for Normal Track and Turnout Passages. In Proceedings of the 9th International Conference on Structural Dynamics (Eurodyn 2014), Porto, Portugal, 30 June–2 July 2014; pp. 827–833.
29. Oregui, M.; Li, S.; Nunez, A.; Li, Z.; Carroll, R.; Dollevoet, R. Monitoring bolt tightness of rail joints using axle box acceleration measurements. *Struct. Control Health Monit.* **2017**, *24*, e1848. [CrossRef]
30. Molodova, M.; Oregui, M.; Nunez, A.; Li, Z.L.; Dollevoet, R. Health condition monitoring of insulated joints based on axle box acceleration measurements. *Eng. Struct.* **2016**, *123*, 225–235. [CrossRef]
31. Salvador, P.; Naranjo, V.; Insa, R.; Teixeira, P. Axlebox accelerations: Their acquisition and time-frequency characterisation for railway track monitoring purposes. *Measurement* **2016**, *82*, 301–312. [CrossRef]
32. Cantero, D.; Basu, B. Railway infrastructure damage detection using wavelet transformed acceleration response of traversing vehicle. *Struct. Control Health Monit.* **2015**, *22*, 62–70. [CrossRef]
33. Quirke, P.; Cantero, D.; OBrien, E.J.; Bowe, C. Drive-by detection of railway track stiffness variation using in-service vehicles. *Proc. Inst. Mech. Eng. Part F J. Rail Rapid Transit* **2017**, *231*, 498–514. [CrossRef]
34. Brien, E.J.O.; Bowe, C.; Quirke, P.; Cantero, D. Determination of longitudinal profile of railway track using vehicle-based inertial readings. *Proc. Inst. Mech. Eng. Part F J. Rail Rapid Transit* **2017**, *231*, 518–534. [CrossRef]
35. Odashima, M.; Azami, S.; Naganuma, Y.; Mori, H.; Tsunashima, H. Track geometry estimation of a conventional railway from car-body acceleration measurement. *Mech. Eng. J.* **2017**, *4*. [CrossRef]
36. Malekjafarian, A.; OBrien, E.; Quirke, P.; Bowe, C. Railway Track Monitoring Using Train Measurements: An Experimental Case Study. *Appl. Sci.* **2019**, *9*, 4859. [CrossRef]
37. Cantero, D.; Arvidsson, T.; OBrien, E.; Karoumi, R. Train-track-bridge modelling and review of parameters. *Struct. Infrastruct. Eng.* **2016**, *12*, 1051–1064. [CrossRef]
38. Zhai, W.M.; Wang, K.Y.; Cai, C.B. Fundamentals of vehicle-track coupled dynamics. *Veh. Syst. Dyn.* **2009**, *47*, 1349–1376. [CrossRef]
39. Lu, F.; Kenned, D.; William, F.W.; Lin, J.H. Symplectic analysis of vertical random vibration for coupled vehicle-track systems. *J. Sound Vib.* **2008**, *317*, 236–249. [CrossRef]

40. Nguyen, K.; Goicolea, J.M.; Galbadon, F. Comparison of dynamic effects of high-speed traffic load on ballasted track using a simplified two-dimensional and full three-dimensional model. *Proc. Inst. Mech. Eng. Part F J. Rail Rapid Transit* **2014**, *228*, 128–142. [CrossRef]
41. Zhai, W.M.; Wang, K.Y.; Lin, J.H. Modelling and experiment of railway ballast vibrations. *J. Sound Vib.* **2004**, *270*, 673–683. [CrossRef]
42. Lei, X.; Noda, N.A. Analyses of dynamic response of vehicle and track coupling system with random irregularity of track vertical profile. *J. Sound Vib.* **2002**, *258*, 147–165. [CrossRef]
43. Sun, Y.Q.; Dhanasekar, M. A dynamic model for the vertical interaction of the rail track and wagon system. *Int. J. Solids Struct.* **2002**, *39*, 1337–1359. [CrossRef]
44. Lou, P. Finite element analysis for train-track-bridge interaction system. *Arch. Appl. Mech.* **2007**, *77*, 707–728. [CrossRef]
45. Goicolea Ruigómez, J.M. *Unofficial Description of Loads and Masses of High Speed Train in Spanish Network AVE S-103 (Siemens ICE3 Velaro)*; E.T.S.I. Caminos, Canales y Puertos (UPM): Madrid, Spain, 2014.
46. Kaynia, A.M.; Park, J.; Noren-Cosgriff, K. Effect of track defects on vibration from high speed train. In Proceedings of the International Conference on Structural Dynamics (Eurodyn 2017), Rome, Italy, 10–13 September 2017; pp. 2681–2686.